APPLIED GEOPHYSICS, Vol.14, No.2 (June 2017), P. 205–215, 9 Figures.
DOI:10.1007/s11770-017-0614-0

Nuclear magnetic resonance T_2 spectrum: multifractal characteristics and pore structure evaluation*

Yan Jian-Ping♦[1,2], He Xu[2], Geng Bin[3], Hu Qin-Hong[4], Feng Chun-Zhen[5], Kou Xiao-Pan[5], and Li Xing-Wen[5]

Abstract: Pore structure characteristics are important to oil and gas exploration in complex low-permeability reservoirs. Using multifractal theory and nuclear magnetic resonance (NMR), we studied the pore structure of low-permeability sandstone rocks from the 4th Member (E_{S4}) of the Shahejie Formation in the south slope of the Dongying Sag. We used the existing pore structure data from petrophysics, core slices, and mercury injection tests to classify the pore structure into three categories and five subcategories. Then, the T_2 spectra of samples with different pore structures were interpolated, and the one- and three-dimensional fractal dimensions and the multifractal spectrum were obtained. Parameters α (intensity of singularity) and $f(\alpha)$ (density of distribution) were extracted from the multifractal spectra. The differences in the three fractal dimensions suggest that the pore structure types correlate with α and $f(\alpha)$. The results calculated based on the multifractal spectrum is consistent with that of the core slices and mercury injection. Finally, the proposed method was applied to an actual logging profile to evaluate the pore structure of low-permeability sandstone reservoirs.
Keywords: NMR T_2 spectrum, multifractal, interpolation, pore structure, permeability, sandstone

Introduction

Low-permeability sandstone reservoirs have become important exploration targets despite their low-permeability and complex pore structure. Pore structure includes the geometry, size, distribution, and connectivity of pores and throats in a rock. The magnetic

Manuscript received by the Editor July 14, 2016; revised manuscript received April 22, 2017.
*This work was supported by the National Natural Science Foundation of China (Grant No. 41202110) and Open Fund of State Key Laboratory of Oil and Gas Reservoir Geology and Exploitation (Southwest Petroleum University) (Grant No. PLN201612), the Applied Basic Research Projects in Sichuan Province (Grant No. 2015JY0200) and Open Fund Project from Sichuan Key Laboratory of Natural Gas Geology (Grant No. 2015trqdz07).
1. State Key Laboratory of Oil & Gas Reservoir Geology and Exploitation (Southwest Petroleum University), Chengdu 610500, China.
2. School of Geoscience and Technology, Southwest Petroleum University, Chengdu 610500, China.
3. Institute of Exploration and Development, ShengLi Oil Field, SINOPEC, Dongying 257015, China.
4. Department of Earth and Environmental Science, University of Texas at Arlington, Texas, 76019, USA.
5. Changqing Division of PetroChina Logging Company, Xi'an 718500, China.
♦Corresponding author: Yan Jian-Ping (Email: yanjp_tj@163.com).

resonance T_2 spectrum has a good correlation with the pore and throat radius distribution, the pore structure types can be divided based on the T_2 spectrum and amplitude (Wang and Li, 2008; Tan et al., 2015), so then the classification of reservoir types can be carried out.

Mandelbrot (1977) proposed a pore structure model based on fractals. Fractal geometry focuses on complex self-similarities. Self-similarity means that the entire or part of a graphic has a similar shape. Typical fractal graphics are the VonKoch curve, coastlines, and the periphery of clouds. The interior of reservoir rocks is complex because it is anisotropic and heterogeneous and has pore fractal characteristics (Pfeifer and Avnir, 1983). The pore volume distribution, throat shape, and fractures all have self-similarities; thus, fractal theory, especially fractal dimensions, has been used to characterize the complex pore structure. Dimension is a mathematical concept that describes the size of a set in space. The ideal spherical model has homogeneous pores and dimension of three. Rocks have a complex pore surface and distribution with fractal characteristics (Pape et al., 1982; Avnir et al., 1984; Katz and Thompson, 1985), which was attributed to diagenesis by Krohn (1988). Fractal dimensions, such as the Hausdorff dimension, box dimension, and multifractal spectrum, can be used to characterize fractal geometries. The Hausdorff dimension is mathematically rigorous but hard to calculate, whereas the calculation of the box dimension is simple and common (Falconer, 1985; Tsakiroglou and Fleury, 1999; Li and Zheng, 2015). The pore structure of reservoir rocks, with fractal characteristics, is obtained by the nitrogen adsorption experiments (Pfeifer and Avnir, 1983).

The three-dimensional fractal dimensions of rocks with different pore structure types have been determined by mercury injection, NMR T_2 spectroscopy, and scanning electron microscopy (Angulo et al., 1992; Krohn, 1988; Zhou and Kang, 2016; Zhou et al., 2016), and their 3D fractal dimensions are between 2 and 3. Using the simple box dimension, the one-dimensional box dimension of rocks with different pore structure types can be obtained from CT images (Peng et al., 2011; Xu, 2014). The vertical heterogeneity of reservoirs is obtained from the box dimension of logging curves (Subhakar and Chandrasekhar, 2016). The box dimension is 1−2. In addition to the single fractal dimension of pore structures, multifractal CT images have been used to study the heterogeneity of carbonate rocks, and it was found that multifractal spectra have continuous distribution anisotropy in 3D space (Xie et al., 2015).

Nuclear magnetic resonance is commonly used in the oil industry (Volokitin et al., 2001; Yun et al., 2002; Ge et al., 2015). However, the researches focus on the pseudocapillary pressure to evaluate the pore structure (Zhang et al., 2007; Xiao and Zhang, 2008). In this study, we used fractal theory and rocks from the 4th Member of the Shahejie Formation in the south slope of the Dongying Sag to study the pore structure. We divided the pore structure into types, calculated the fractal dimensions of the T_2 spectrum, and inferred that the differences in the fractal dimensions of the T_2 spectrum of the different pore structures reflect the different pore structure types and can be used to distinguish them. A single dimension could not completely describe the multiscale pore structure using the T_2 spectrum. Consequently, multifractal computation of the T_2 spectrum was carried out. The multifractal parameters are the intensity of singularity α and the distribution of density $f(\alpha)$. The use of multifractal parameters can help in the evaluation of pore structure and the identification of reservoirs.

Theory

In rocks, the pore distribution, throat shape, and fractures have self-similarities; therefore, fractal theory and especially fractal dimensions are used to represent the pore structure. The box dimension is commonly used (Falconer, 1985) owing to its computational simplicity. The box dimension is defined as follows: a square box with side length δ covers a plane set M, and the intersection number $n(M)_\delta$ between the box and the set M is calculated. With decreasing δ, $n(M)_\delta$ increases, and $\delta \to 0$, the slope of $n(M)_\delta$, is calculated and $-\log(\delta)$ in the log–log coordinates of M. The dimensions are obtained by using cubes with side length δ.

The use of power-law functions, such as $y(x) = cx^a$, where $y(x)$ is the dependent variable and c and a are constants, is common. By assuming a set of F for $\delta > 0$, we can exclude the irregularities below δ and observe the variation of $M(F)$ when $\delta \to 0$. If the two nonnegative constants c and s lead to $M(F)_\delta \propto c\delta^{-s}$, then F has dimension s, and c is its length. The rough surface of rocks has self-similar characteristics as well as the pore distribution (Hansen et al., 1988). Therefore, mercury injection and T_2 spectrum are used in fractal analysis.

There is a statistical instead of mathematical similarity in a complex fractal phenomenon. The fractal dimensions change with observation scale; therefore,

multifractals are used to represent this kind of change. The mathematical definition is as follows: when the distribution of measure μ is discussed in the fractal set F, F is divided into several elements in δ scale. If $\mu_i \propto \delta^{\alpha_i}$ (μ_i is the ith element average value of μ), α is the intensity of singularity. If several elements have the same intensity of singularity, μ is represented by $\mu(\alpha)$. F_α is a subset of elements with the same intensity of singularity, and its s-dimensional fractal dimension (Wen, 2003) is

$$H^s\left(F_\alpha, \mu(\alpha)\right) = \lim_{\delta \to 0} H^s{}_\delta\left(F_\alpha, \mu(\alpha)\right). \quad (1)$$

The set is covered by box measures with side length L, and $P_i(L)$ is the probability for the ith box which fits the equation (Chhabra and Jensen, 1989)

$$P_i(L) \sim L^{\alpha_i}. \quad (2)$$

When the box number is $N(\alpha)$, the intensity of singularity of P_i is between α and $\alpha + d\alpha$. $f(\alpha)$ is the Hausdorff dimension, and the density of distribution is (Chhabra and Jensen, 1989)

$$N(\alpha) \sim L^{-f(\alpha)}. \quad (3)$$

The relation between the generalized dimension D_q of the qth measure and the intensity of singularity α is (Chhabra and Jensen, 1989)

$$D_q = \frac{1}{q-1} \lim_{L \to 0} \frac{\log \sum_i p_i^{q(L)}}{\log L}. \quad (4)$$

If $f(\alpha)$ and D_q are smooth functions of α and q, $f(\alpha)$ is obtained from the quality index number $\tau(q) = (q-1)D_q$ by Legendre transformation (Chhabra and Jensen, 1989). In rocks with macro- and meso- to micropores, different scales have different fractal features. CT images are used to build the probability density function to describe the micropore characteristics. The relation is also constructed by using core slices, mercury-injection data, and nuclear magnetic resonance T_2 spectra.

One- and three-dimensional fractal characteristics of the T_2 spectrum

We statistically analyzed capillary pressure, core slices, and nuclear magnetic resonance data from the 4th Member of the Shahejie Formation at the south slope of Dongying Sag slope (Table 1) and described the one- and three-dimensional fractal characteristics of the T_2 spectrum.

Table 1 4th Member, Shahejie Formation porosity data

Pore structure types	Lithology	Reservoir validity type	Por. (%); Perm (mD)	Mercury injection P_d (Mpa); SHg_{max} (%)	Nuclear magnetic resonance T_{2cut} (ms); S_{BVI} (%)	Reservoir type
I_1	Siltstone Fine sandstone	Effective reservoir	Por. ≥ 15 Perm ≥ 10	P_d < 0.2 SHg_{max} ≥ 80	T_{2cut} ≥ 14 S_{BVI} come near 50%	Medium porosity low permeability
I_2	Siltstone Fine sandstone	Effective reservoir	Por. ≥ 15 1≤ Perm< 10	0.2 ≤ P_d < 0.4 70 ≤ SHg_{max} < 80	T_{2cut} ≥ 14 SBVI come near 50%	Medium porosity extra-low permeability
II_1	Siltstone Tuffaceous siltstone	Effective reservoir	10 ≤ Por. < 15 0.3 ≤ Perm < 1	0.4 ≤ P_d < 0.7 60 ≤ SHg_{max} < 70	10 ≤ T_{2cut} <14 50 ≤ S_{BVI} < 75	Low porosity ultra-low permeability
II_2	Argillaceous siltstone Tuffaceous siltstone	Poor reservoir	7 ≤ Por. < 10 0.1 ≤ Perm < 0.3	0.7 ≤ P_d < 1.6 50 ≤ SHg_{max} < 60	T_{2cut} < 10 ms 75 ≤ S_{BVI} < 85	Extra-low porosity ultra-low permeability
III	Mudstone Argillaceous siltstone	Non-reservoir	Por. < 7 Perm < 0.1	P_d ≥ 1.6 SHg_{max} < 50	T_{2cut} < 10 S_{BVI} ≥ 85	Ultra-low porosity non-permeability

Notes: Pd (Mpa): displacement pressure is the mercury pressure of the maximal pore throat; SH_{gmax} (%): relative maximal mercury volume; S_{BVI} (%): relative irreducible fluid volume; T_{2cut} (ms): transverse relaxation time when the cumulative total porosity in the noncentrifugal T_2 spectrum equals the irreducible fluid porosity.

One-dimensional fractal characteristics

The NMR T_2 spectrum is a curve on a plane. The original data are echoes, and the echo amplitude decreases with time. The T_2 spectrum is the two-dimensional curve obtained by the multiexponential inversion of the original echoes. The abscissa is the transverse relaxation time, and the ordinate is the corresponding echo amplitude. Different tracing patterns represent different pore structures that could be expressed by using box dimensions.

Considering the porosity types in the study area, type-I T_2 spectrum represents large pores and throats. Type-II T_2 spectrum represents medium-sized pores, and type-III T_2 spectrum denotes the smaller pores. Figure 1 shows the T_2 spectra. For water-saturated rocks, the T_2 spectrum correlates with the pore size distribution in the logarithmic scale but not in the linear scale (Xiao, 2007). Because of the nonuniform distribution of the T_2 spectra, we need to interpolate to avoid the error in the pore structure analysis. Thus, we calculate the logarithm of the T_2 spectrum and perform linear interpolation. Three types of box dimensions (Table 2) are obtained from the T_2 spectrum that clearly decreases from type I to III.

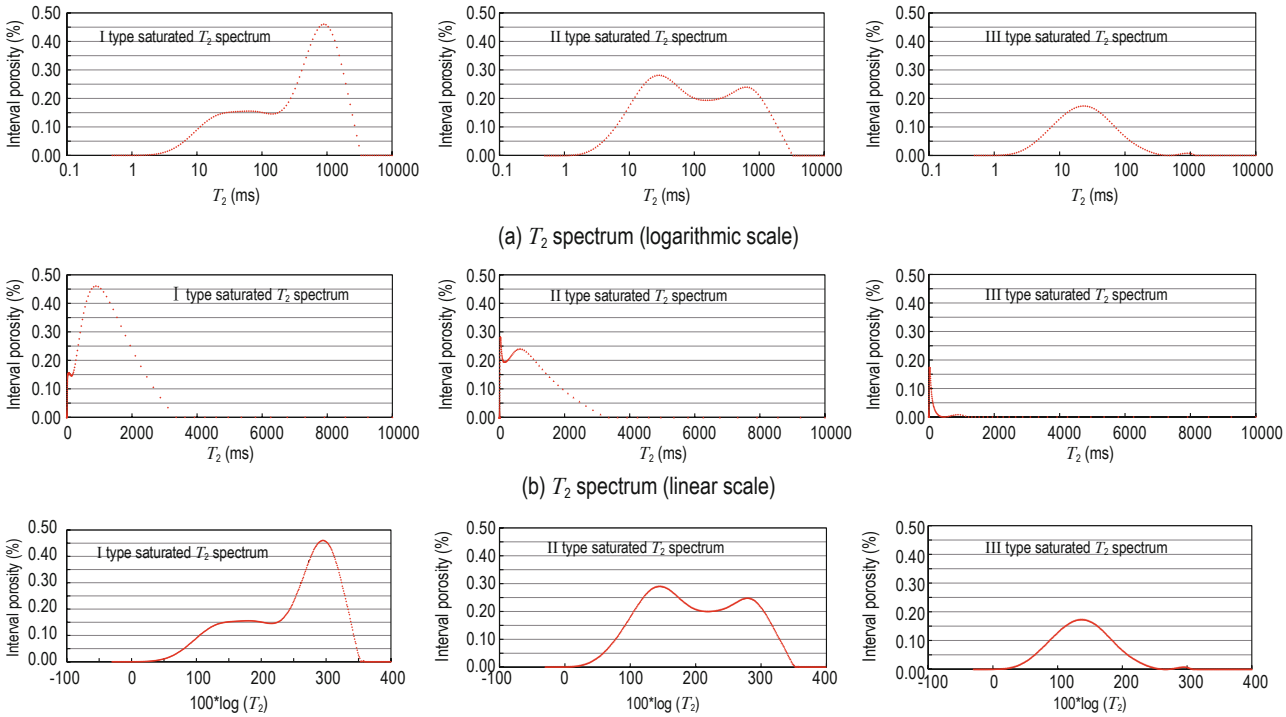

(a) T_2 spectrum (logarithmic scale)

(b) T_2 spectrum (linear scale)

(c) T_2 spectrum (interpolation)

Fig.1 Pore structure and T_2 spectra.

Table 2 Box dimensions of different pore structures

Pore structure type	Pore (%)	Permeability (mD)	Box dimensions
I	17.12	8.22	1.0323
II	11.46	0.36	1.0267
III	5.87	0.01	1.0146

Three-dimensional fractal characteristics

The T_2 spectrum from NMR contains pore structure information and is used to build pseudocapillary pressure curves (Volokitin et al., 2001; Yun et al., 2002; Zhang, et al., 2007).

$$S_v = \left[\frac{T_{2\max}}{T_2}\right]^{D-3}, \qquad (5)$$

and is transformed to

$$\lg(S_v) = (3-D)\lg(T_2) + (D-3)\lg T_{2\max}, \qquad (6)$$

where T_2 is the transverse relaxation time (ms), S_v is the proportion of pore volume below the corresponding T_2 in total pore volume, D is the fractal dimension, and $T_{2\max}$ is the maximum of the transverse relaxation time.

lg(Sv) and lg(T_2) are linearly correlated in rocks with fractal characteristics. The three-dimensional fractal dimension D (Table 3) is obtained by regression analysis (Figure 2) of T_2 spectrum data. D could be used to characterize the different pore structure types.

The three-dimensional fractal dimension changes with pore structure; however, the fractal dimension is not sensitive to the pore structure. Presumably, a single dimension cannot describe multiscale pore structures. Thus, the pore structure is studied by using multifractals.

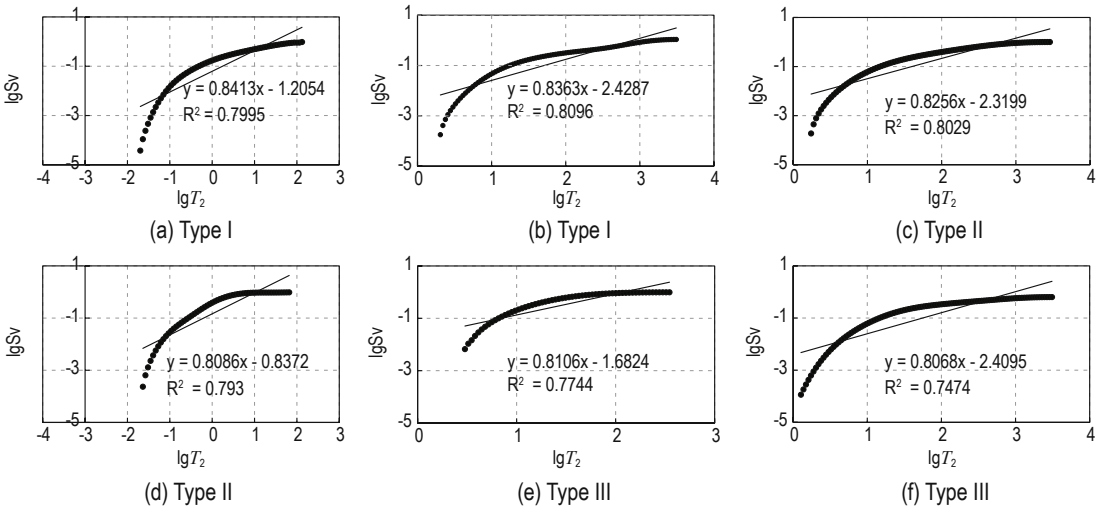

Fig.2 S_v vs T_2 for different pore structure types.

Table 3 Fractal dimensions of different pore structure types

Pore structure type	Sample number	Fractal dimension D	Dimension average $\overline{D}$	Coefficient of association R
I	(a)	2.159	2.161	0.894
I	(b)	2.164	2.161	0.899
II	(c)	2.175	2.183	0.896
II	(d)	2.192	2.183	0.891
III	(e)	2.190	2.192	0.880
III	(f)	2.193	2.192	0.864

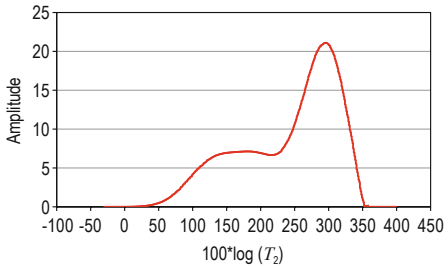

Fig.3 Interpolation of the T_2 spectrum.

Pore structure and T_2 multifractal spectrum

Multifractal characteristics of the T_2 spectrum

Irreducible fluids have different NMR T_2 responses in rocks, and irreducible fluids in small pores have ultrashort transverse relaxation time compared with free-moving fluids. Modern MRI instruments are capable of retrieving pore fluid data (Xiao, 2007) and total porosity. The T_2 spectrum yields more pore structure information than mercury-injection test data. We thus use the spectrum dimension to characterize the pore structure.

The T_2 spectrum also requires interpolation (Figure 3) and multifractal calculations. Based on Chhabra and Jensen (1989), a functional image in plane $G\,f(q)$ is described by

$$f(q)=\lim_{r\to 0}\frac{\sum_i \mu_i(q,r)\ln\left[\mu_i(q,r)\right]}{\ln r}, \qquad (7)$$

$$\alpha(q)=\lim_{r\to 0}\frac{\sum_i \mu_i(q,r)\ln\left[p_i(r)\right]}{\ln r}, \qquad (8)$$

where r is the degree of the box dimension, $p_i(r)$ is the probability of the box of tab i

$$\mu_i(q,r)=\frac{\left[p_i(r)\right]^q}{\sum_i\left[p_i(r)\right]^q}, \qquad (9)$$

$$p_i\left(r^{(n)}\right)=\frac{S_i^{(n)}}{S^{(n)}}, \qquad (10)$$

where G could be covered by n boxes D_i with measure $r^{(n)}$, when n is sufficiently large, $p_i\left(r^{(n)}\right)=\frac{S_i^{(n)}}{S^{(n)}}$ and $S_i^{(n)}$ is the length of $G\cap D_i^{(n)}$, and $S^{(n)}$ is the length of G in this scale.

We used the above equations to estimate the multifractal T_2 spectrum (Figure 4), and the estimated parameters are listed in Table 4. With increasing order from $q_{\min}$ to $q_{\min}$, α decreases. $f(\alpha)$ increases until q =

0, and then, $f(\alpha)$ decreases (Figure 4). The multifractal spectrum is a parabola without an axis of symmetry, the left wing is longer of which $q > 0$ and the right wing is shorter of which $q < 0$ but with an inflection point at $q = 0$. The abscissa is α (intensity of singularity), and the ordinate is $f(\alpha)$ (density of distribution).

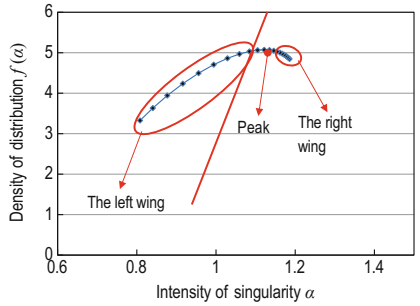

Fig.4 Multifractal of the T_2 spectrum.

Multifractal spectrum and pore structure

The multifractal spectrum consists of two parts: $q > 0$ and $q < 0$. When $q > 0$, $\mu_i(q, r)$ is small, and for $q > 0$, $\mu_i(q, r)$ is high.

Different pore structures in rocks have different T_2 spectral shapes. Two samples with different porosity, permeability, and T_2 spectral shapes are selected (Figures 5). First, the differences are observed in the intensity of singularity. Rocks with high porosity, many large pores, and high permeability have consequently high α in T_2 spectrun. In contrast, rocks with low porosity, small number of large pores, and low permeability have small α.

Table 4 Multifractal data for the T_2 spectrum

q	α	$f(\alpha)$	q	α	$f(\alpha)$
−10	1.185673	4.845948	1	1.10504	5.063226
−9	1.183019	4.871128	2	1.084376	5.031868
−8	1.179973	4.896981	3	1.0591	4.968275
−7	1.176444	4.923402	4	1.028929	4.862269
−6	1.172314	4.950195	5	0.994177	4.705536
−5	1.167425	4.977011	6	0.955953	4.495084
−4	1.161573	5.003258	7	0.91612	4.236126
−3	1.154483	5.027954	8	0.876927	3.942325
−2	1.1458	5.049512	9	0.840454	3.632604
−1	1.135063	5.065424	10	0.808142	3.326026
0	1.1217	5.07186			

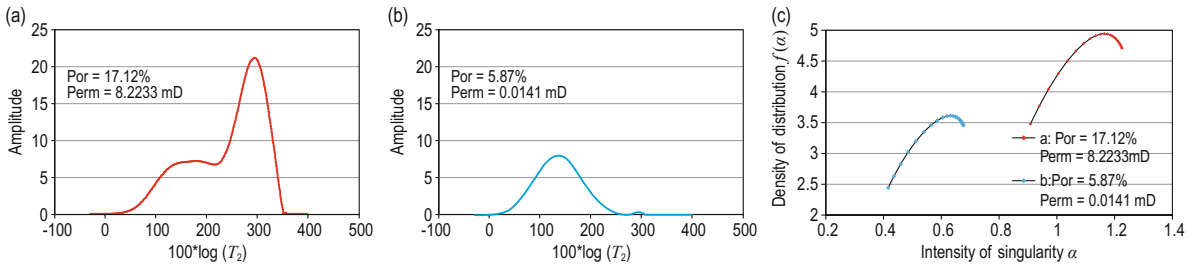

Fig.5 Multifractal T_2 spectrum of (a) high porosity and permeability, (b) low porosity and permeability, and (c) multifractal spectrum.

We selected a low-permeability beach bar sandstone from the 4th Member of the Shahejie Formation in the south slope of the Dongying Sag. Nuclear magnetic resonance and test data are from the FX Well. Samples 1 and 2 are type I, samples 3, 4, and 5 are type II, and samples 6, 7, and 8 are type III. Their corresponding interpolated T_2 spectra are shown in Figure 6. The multifractal spectra of the samples are shown in (Figure 7), and the parameters are given in Table 5. Clearly, different pore structures have different multifractal spectra. For $q < 0$, the high intensity of singularity α correlates with high porosity and permeability. In type I, α is 1.12–1.23, and $f(\alpha)$ is 4.71–5.07. In type II, α is 0.95 –1.14, and $f(\alpha)$ is 3.75–4.17. In type III, α is 0.63–0.84, and $f(\alpha)$ is 3.46–3.83 (Figures 7b and 7c).

The sandstone of E_{S4} Formation contains calcite, feldspar, and lithic fragments.The dissolution has created type-I pore structures (Figures 8a–8d, Table 6, samples 1 and 2). The rock samples were analyzed by mercury injection test, the maximum mercury injection saturation is 70%–80%, the displacement pressure is below 0.4 MPa, α (intensity of singularity) is 1.12–1.23, and $f(\alpha)$ (density of distribution) is 4.71–5.07 (Table 6).

Compaction and cementation created type-II pore structures (Figures 8e–8j, samples 3, 4, and 5), the maximum mercury injection saturation is 40%–70%, the displacement pressure is 0.4–1.6 MPa, α (intensity of singularity) is 0.95–1.14, and $f(\alpha)$ (density of distribution) is 3.75–4.17 (Table 6). Rocks with a type-III pore structure are compacted and affected by

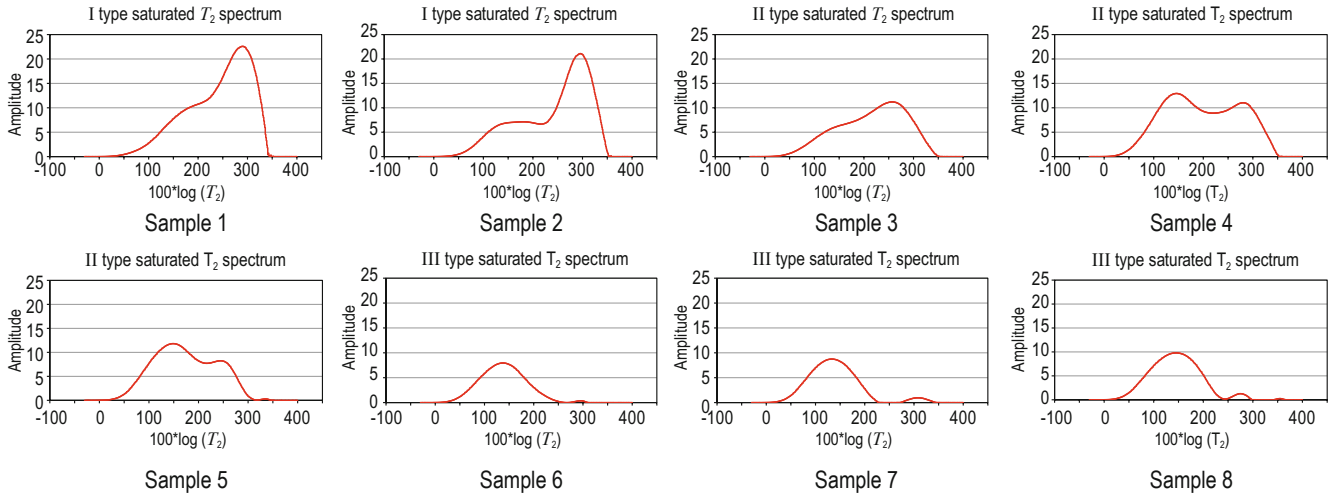

Fig.6 Interpolated T_2 spectra of different pore structures.

Table 5 Multifractal parameters for different pore structure types

Sample number	1		2		3		4		5		6		7		8	
Porosity (%)	17.12		19.42		14.13		11.46		12.66		7.74		5.18		5.87	
Permeability (mD)	8.2233		2.7722		0.4741		0.3627		0.1323		0.0399		0.0139		0.0141	
q	α	$f(\alpha)$	A	$f(\alpha)$	α	$f(\alpha)$	α	$f(\alpha)$	α	$f(\alpha)$	A	$f(\alpha)$	α	$f(\alpha)$	α	$f(\alpha)$
−10	1.23	4.71	1.19	4.85	1.14	4.03	1.04	3.81	1.04	3.75	0.84	3.65	0.72	3.57	0.68	3.46
−9	1.22	4.74	1.18	4.87	1.14	4.05	1.03	3.84	1.04	3.78	0.84	3.67	0.72	3.59	0.67	3.47
−8	1.22	4.77	1.18	4.90	1.13	4.07	1.03	3.86	1.03	3.81	0.84	3.69	0.71	3.60	0.67	3.49
−7	1.22	4.80	1.18	4.92	1.13	4.08	1.03	3.88	1.03	3.85	0.84	3.70	0.71	3.62	0.67	3.51
−6	1.21	4.83	1.17	4.95	1.13	4.10	1.03	3.90	1.02	3.88	0.84	3.72	0.71	3.64	0.67	3.53
−5	1.21	4.85	1.17	4.98	1.13	4.12	1.02	3.92	1.02	3.92	0.83	3.75	0.71	3.65	0.66	3.55
−4	1.20	4.88	1.16	5.00	1.12	4.13	1.02	3.94	1.01	3.95	0.83	3.77	0.70	3.67	0.66	3.56
−3	1.19	4.90	1.15	5.03	1.12	4.15	1.01	3.96	1.00	3.99	0.82	3.79	0.70	3.68	0.66	3.58
−2	1.19	4.92	1.15	5.05	1.11	4.16	1.01	3.97	0.99	4.02	0.81	3.81	0.69	3.70	0.65	3.60
−1	1.18	4.94	1.14	5.07	1.11	4.17	1.00	3.98	0.97	4.05	0.80	3.83	0.69	3.71	0.64	3.61
0	1.16	4.94	1.12	5.07	1.10	4.17	0.99	3.99	0.95	4.06	0.79	3.83	0.68	3.71	0.63	3.61

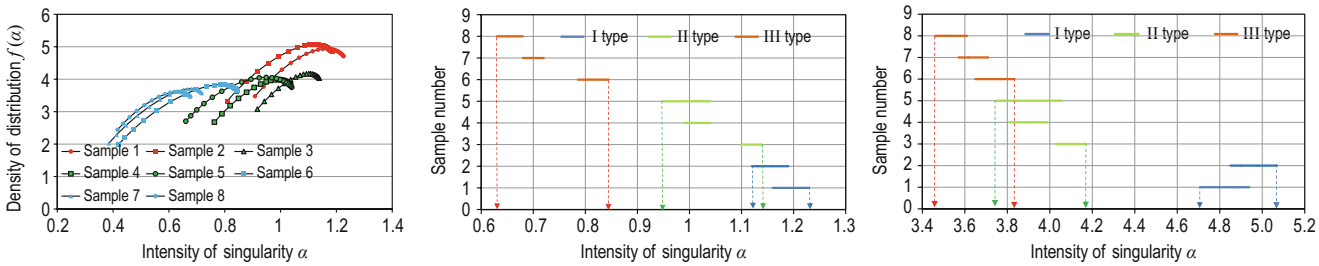

(a) Multifractal spectrum (b) Intensity of singularity (c) Density of distribution

Fig.7 Multifractal spectrum and parameter distribution.

cementation (Figures 8k–8p, samples 6, 7, and 8). The maximum mercury injection saturation is less than 50%, the displacement pressure is greater than 1.6 MPa, α (intensity of singularity) is 0.63–0.84, and $f(\alpha)$ (density of distribution) is 3.46–3.83 (Table 6). As the pore structure of rock becomes worse, the corresponding maximum mercury saturation gradually decreases, and the displacement pressure increases gradually. The multifractal analysis is consistent with the mercury injection data. The classification of pore structure types based on multifractal parameters is further proved to be practical and effective.

Multifractal characteristics and pore structure evaluation

Table 6 Multifractal and mercury injection parameters of different pore structure types

Sample number	1	2	3	4	5	6	7	8
Pore structure type	I	I	II	II	II	III	III	III
Displacement pressure (MPa)	0.20	0.38	0.45	1.62	1.02	1.67	1.96	1.8
Maximum mercury injection saturation (%)	80.93	72.41	71.38	54.98	67.46	40.90	46.25	27.34
Median pressure (MPa)	1.42	4.22	4.80	23.02	14.84	\	\	\
Intensity of singularity α	1.16–1.23	1.12–1.19	1.10–1.14	0.99–1.04	0.95–1.04	0.79–0.84	0.68–0.72	0.63–0.68
Range of α	1.12–1.23	1.12–1.23	0.95–1.14	0.95–1.14	0.95–1.14	0.63–0.84	0.63–0.84	0.63–0.84
Density of distribution $f(\alpha)$	4.71–4.94	4.85–5.07	4.03–4.17	3.81–3.99	3.75–4.06	3.65–3.83	3.57–3.71	3.46–3.61
Range of $f(\alpha)$	4.71–5.07	4.71–5.07	3.75–4.17	3.75–4.17	3.75–4.17	3.46–3.83	3.46–3.83	3.46–3.83

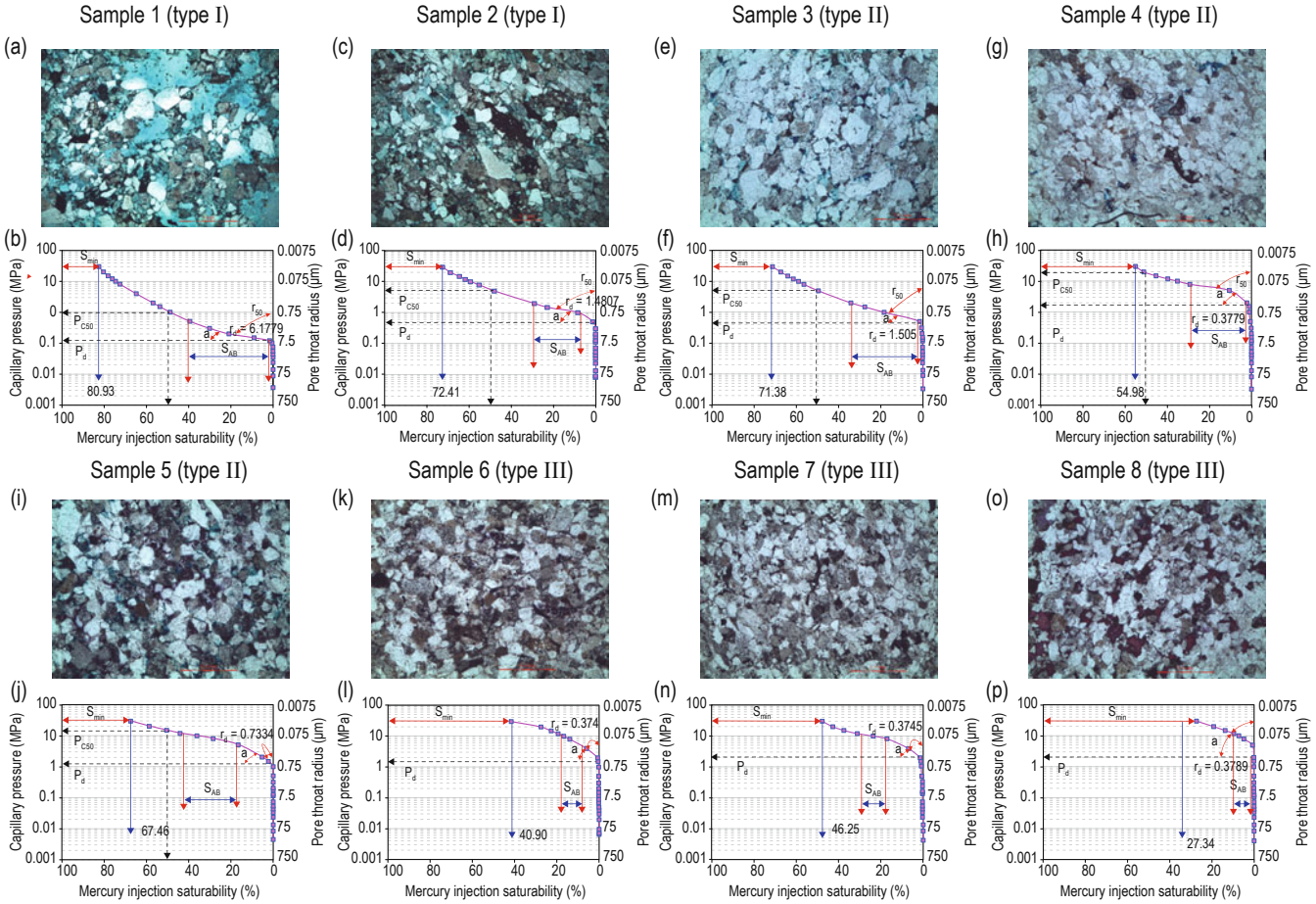

Fig.8 Mercury injection capillary pressure vs pore structure.

Note: P_{C50} (MPa): the pressure when the percent of the mercury volume of the pore volume is 50%; r_d (μm): the radius when the mercury start get in the pore; P_d (MPa): the pressure when the mercury start get in the pore; S_{min} (%): the percent of the mercury volume of the pore volume when the pressure is maximal; S_{AB} (%): the percent of the capillary pressure curve's gently part of the total mercury volume; a: the angle of the capillary pressure curve's gently part.

It is well known that the nuclear magnetic resonance T_2 spectra reflect the pore and throat radius distribution. The pore structure types can be divided based on the T_2 spectrum and amplitude. Comparing the calculation results of the multifractal spectrum, the one-dimensional box dimension, and three-dimensional fractal dimension, we can see that the box dimension and the three-dimensional fractal dimensions for the different structure

types differ a little, in the second decimal after decimal point, so it is impossible to determine the boundary value of the different pore structures. It is different from the conventional mercury injection experiment, building pseudocapillary pressure curves from T_2 spectrum (Xiao and Zhang, 2008), and core slice authentication, after the multi fractal in the T_2 spectrum, the difference of the multifractal parameters is greater, in the first decimal after the decimal point. the pore structure can be quantified by α and $f(\alpha)$.

Instance analysis

Taking the profile of E_{S4} from well F as an example, different pore structure types are chosen for T_2 spectrum multifractal analysis. The statistical analysis suggests that α and $f(\alpha)$ (Figure 9) are consistent with experimental results when $q<0$. The differences in α are attributed to the differences in the fluid composition. The variation trend is consistent with that calculated by NMR T_2 spectra

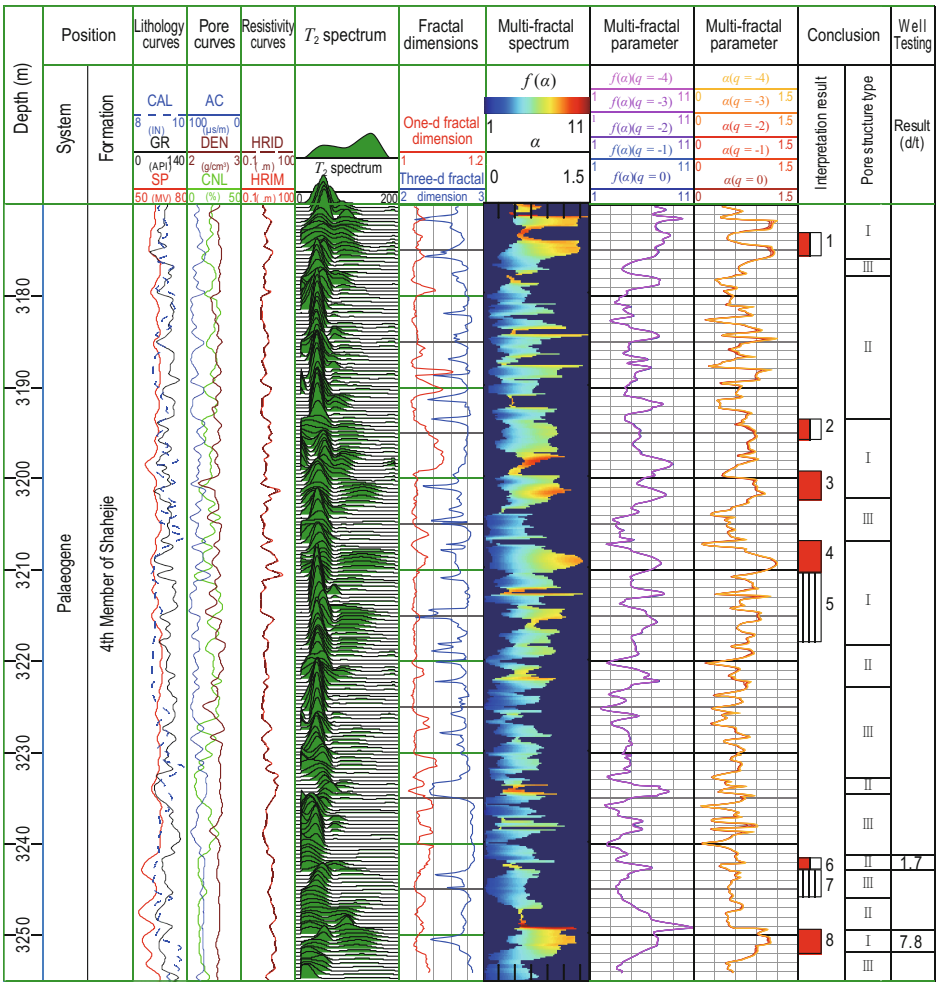

Fig.9 Fractal analysis and interpretation for Well F.

Fluids in different states have different transverse relaxation contributions from surface relaxation and diffusion relaxation (Hu et al., 2016). In other words, different fluids have different transverse relaxation response characteristics. Gas has a lower hydrogen index, which leads to lower transverse relaxation time and amplitude. Light oil and water have similar hydrogen indices and transverse relaxation response characteristics; therefore, water and oil are polarized and have long waiting times and echo spacing. For oil and water, the T_2 spectra of similar pore structure types have similar shapes, whereas different pore structure types have different shapes.

The reservoirs of the Shahejie Formation in Dongying Sag are mostly filled with light oil. The oil and water signal overlap and can be used to decipher the different

pore structures. Therefore, the multifractal of the T_2 spectrum could be used to analyze and divide the pore structure types.

Type-I pore structure (3250–3252 m) has high porosity and permeability, with α average value of 0.8447, box dimension average value of 1.03, and three-dimensional fractal dimension average value of 2.62. These data represent an oil-bearing bed with 7.8 t/d production. Type-II pore structure (3241.5–3242.75 m) has relative low porosity and permeability, with α average value of 0.6355, box dimension average value of 1.06, and three-dimensional fractal dimension average value of 2.72. The data represent an oil-bearing interval of 1.7 t/d production. Type-III pore structure (3242–3244 m) has relative low porosity and permeability, with α average value of 0.4421, box dimension average value of 1.0415, and three-dimensional fractal dimension average value of 2.73. Therefore, parameters α and $f(\alpha)$ can be used to distinguish the different pore structure types in well profiles. Multifractals are an attribute of the T_2 spectrum, and multifractal analysis of nuclear magnetic resonance logging in complex low-permeability sandstone can be used to evaluate the pore structure of reservoirs.

Conclusions

One- and three-dimensional fractal dimensions could be used to classify different pore structure types. Different pore structures have different multifractal characteristics that are expressed in the shape of the multifractal spectrum and parameters α (intensity of singularity) and $f(\alpha)$ (density of distribution). Rocks with high porosity and permeability have high α and $f(\alpha)$, whereas rocks with low porosity and permeability have small α and $f(\alpha)$. For $q<0$, the multifractal parameters can describe the T_2 spectrum in detail.

In nonheavy oil reservoirs without gas, nuclear magnetic resonance T_2 spectra can express the differences among different pore structure types based on α and $f(\alpha)$. The proposed method was applied to low-permeability sandstone reservoir with good results.

Acknowledgments

We would also like to thank Hu Falong and Tan Maojin for the constructive suggestions that significantly improved the manuscript.

References

Angulo, R. F., Alvaraso, V., and Gonzalea, H., 1992, Fractal dimensions from mercury intrusion capillary tests: The Second Latin American Petroleum Engineering Conference, II LAPEC, of the Society of Petroleum Engineers, SPE 23695, 255–263.

Avnir, D., Farin D., and Pfeifer P., 1984, Molecular fractal surfaces: Nature, **308**(5956), 261–263.

Chhabra, A., and Jensen, R. V., 1989, Direct determination of the $f(\alpha)$ singularity spectrum: Physical Review Letters, **62**(12), 1327–1330.

Falconer, K. J., 1985, The geometry of fractal sets: Cambridge, England.

Ge, X. M., Fan, Y. R., Li, J. T., et al., 2015, Pore structure characterization and classification using multifractal theoryAn application in Santanghu basin of western China: Journal of Petroleum Science and Engineering, **127**, 297–304.

Hansen, J. P., and Skjeltorp, A. T., 1988, Fractal pore space and rock permeability implications: Physical Review B, **38**(4), 2635–2638.

He, Y. D., Mao,Z. Q., Xiao, L. Z., et al., 2005, An improved method of using NMR T_2 distribution to evaluate pore size distribution: Chinese Journal of

Hu, F. L, Zhou, C., Li, C. L., et al., 2016, Water spectrum method of NMR logging for identifying fluids: Petroleum Exploration and Development, **43**(2), 244–252.

Katz, A. J., and Thompson, A. H., 1985, Fractal sandstone pores: Implications for conductivity and pore formation: Physical Review Letters, **54**(12), 1325–1328.

Krohn, C. E., 1988, Sandstone fractal and euclidean pore volume distributions: Journal of Geophysical Research-Solid Earth and Planets, **93**(B4), 3286–3296.

Li, J. H., and Zheng B., 2015, A New method for fractal characterization of microscopic pores and its application in shale reservoirs: Natural Gas Industry, 2015, **35**(5), 52–59.

Mandelbrot, B. B., 1977, Fractals: Form, Chance and Dimension, San Francisco, W. H. Freeman.

Pape, H., Riepe, L., and Schopper, J. R., 1982, A pigeon-holemodel for relating permeability to specific surface: The Log Analyst, **23**(1), 5–13.

Peng, R. D., Yang Y. C., Ju, Y., et al., 2011, Computation of fractal dimension of rock pores based on gray CT images: Chinese Science Bulletin, **56**(26), 2256–2266.

Pfeifer, P., and Avnir, D., 1983, Chemistry in noninteger dimensions between two and three, fractal theory of

heterogenous surface: Journal of Chemical Physics, **79**(7), 3558–3565.

Subhakar, D., and Chandrasekhar, E., 2016, Reservoir characterization using multifractal detrended fluctuation analysis of geophysical well-log data: Physica A, **445**(1), 57–65.

Tan, M. J., Mao, K. Y., Song, X. D., et al., 2015, NMR petrophsical interpretation method of gas shale on core NMR experiment: Journal of Petroleum Science and Engineering, **136**, 100–111.

Tsakiroglou, C. D., and Fleury, M., 1999, Resistivity index of fractional wettability porous media: Journal of Petroleum Science and Engineering, **22**, 253–274.

Volokitin, Y., Looyestigin, W. J., and Slijkerman, W. F. J., et al., 2001, A practical approach to obtain primary drainage capillary pressure curves from NMR core and log data: Petrophysics, **42**(4), 334–343.

Wang, K.W., and Li, N., 2008, Numerical simulation of rock pore throat structure effects on NMR T2 distribution, Applied Geophysics, **5**(2), 86–91.

Wen, H. M., 2003, Study of Fractal Log Interpretation Theory and Method: PhD Thesis, Chengdu University of Technology, Chengdu.

Xiao, L. Z., 2007, Frontiers Investigation in Well Logging Science: Petroleum Industry Press, Beijing.

Xiao, L. Z., and Zhang, W., 2008, A new method to construct reservoir capillary pressure curves using NMR log data and its application: Applied Geophysics, **5**(2), 92–98.

Xie, S. Y., He, Z. L., Qiang, Y. X., et al., 2015, Multifractality of 3D pore structures of carbonate rocks based on CT images: Journal of Geology, **39**(1), 4653.

Xu, Z. X., 2014, Heterogeneity of shale reservoirs based on CT images: Lithologic Reservoirs, **26**(6), 46–49.

Yun, H. Y., Zhao, W. J., Liu, B. K., et al., 2002, Researching Rock Pore Structure with T2 Distribution: Well Logging Technology, **26**(1), 18–21.

Zhang, C. M., Chen, Z. B., Zhang, Z. S., et al., 2007, Fractal Characteristics of Reservoir Rock Pore Structure based on NMR T_2 Distribution: Journal of Oil and Gas Technology, **29**(4), 80–86.

Zhou, L., and Kang, Z., 2016, Fractal characterization of pores in shales using NMR: A case study from the Lower Cambrian Niutitang Formation in the Middle Yangtze, Platform, Southwest China: Journal of Natural Gas Science and Engineering, **35**(Part A), 860 –872.

Zhou, S., Liu, D., M., Cai, Y. D., et al., 2016, Fractal characterization of pore–fracture in low-rank coals using a low-field NMR relaxation method: Fuel, **181**, 218–226.

Yan Jian-Ping, associate professor, graduated in 2004 from China University of Petroleum (Hua Dong) with a degree in Exploration Technology and Engineering. Subsequently, he received his master's in Earth Exploration and Information Technology in 2007 and Ph.D. in Marine Geology from Tongji University in 2010. His research interests are rock physics and evaluation of unconventional reservoirs.